CFD MODEL TO ANALYZE SO_2 ABSORPTION IN A SEAWATER DROPLET

(DOI No: 10.3940/rina.ijme.2019.a4.525a)

M I Lamas and **C G Rodriguez**, Universidade da Coruña, Spain

SUMMARY

In the recent years, seawater scrubbers have become an interesting option to reduce SO_2 emissions in marine engines. In this regard, this paper proposes a numerical model to analyze SO_2 absorption in seawater. A single seawater droplet was analyzed, and the developed model was used to predict the influence of several parameters on the desulphurization efficiency, such as the droplet diameter, SO_2 concentration, alkalinity and temperature. It was found that a droplet of 200 µm initial diameter can absorb up to $1.77 \cdot 10^{-14}$ mol of S for the parameters analyzed, and this reduction improves when the alkalinity and SO_2 concentration are increased and diameter, seawater temperature and gas temperature are reduced. Differences up to of 21.5%, 19.8%, 2.2% and 16.3% in the S reduction were obtaining varying the SO_2 initial concentration, alkaline initial concentration, initial liquid temperature and initial gas temperature respectively.

NOMENCLATURE

A	Area (m^2)
ΔG^0	Standard Gibbs free energy change (J/mol)
D	Diameter (m or µm)
ε	Small quantity (m)
ϕ	Level set (m)
h	Heat transfer coefficient (W m^{-2} K)
k	Henry's constant (mol kg^{-1} atm^{-1})
Pr	Prandtl number (-)
R	Universal gas constant (J mol^{-1} K^{-1})
Re	Reynolds number (-)
ρ	Density (kg m^{-3})
σ	Surface tension (N m^{-1})
ξ	Artificial time (s)
T	Temperature (K)
t	Time (s)
u	Velocity (m s^{-1})
υ	Kinematic viscosity (N s m^{-2})

1. INTRODUCTION

Although most combustion systems have achieved a significant reduction of their emissions during the last years, it is necessary to further reduce them due to the increasingly restrictive legislation. Particularly, in the marine field most medium and large marine engines operate on heavy fuel oil, which is a cheap combustible but contains an important quantity of pollutant substances, especially sulphur (S) (Lamas, et al, 2013). The oxidation of sulphur in the fuel forms sulphur oxides (SO_x) in the exhaust gas, especially SO_2 (Lamas, et al, 2015; Lamas & Rodriguez, 2017). SO_x are the mayor source of acid rain (Lamas & Rodriguez, 2013), which causes breathing difficulties, respiratory illnesses, acidification of lakes, agricultural crops, corrosion of materials, etc. In order to prevent these consequences, the International Maritime Organization (IMO) established a set of regulations to reduce emissions. Particularly, Annex VI of MARPOL 73/78 regulates the SO_x emissions by setting a maximum limiting value on the fuel sulphur content. This limit has been reduced from 4.5% to 3.5% from 1 January 2012 and then from 3.5 to 0.5% w/w from 1 January 2020. Besides, there are sulphur emission control areas (SECAs) with more stringent requirements. The sulphur limits and implementation dates required by IMO are illustrated in Figure. 1. Instead of using low sulphur content fuels, other allowed solution is to employ exhaust gas cleaning/after-treatment systems. These have become a promising alternative due to the high price of low sulphur fuels such as Marine Diesel Oil and Marine Gas Oil (Seddiek & Elgohari, 2014).

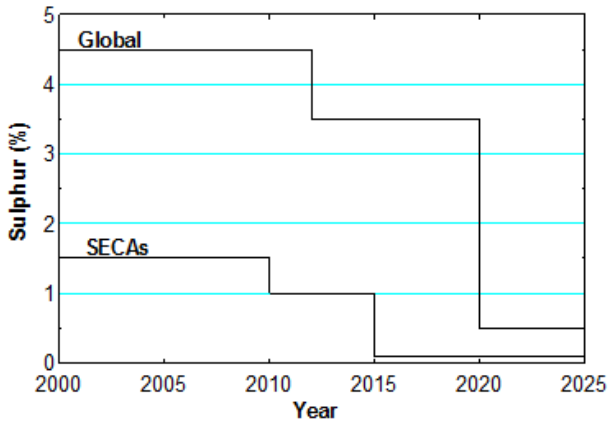

Figure 1. Sulphur limits and implementation dates.

The most common method for flue gas desulphurization is scrubbing through an alkali absorbent like urea (Barbooti, et al, 2011), NaOH (Hikita, et al, 1977), limestone slurry (Lancia, et al, 1997; Puskar, et al, 2013), NaCl (Jeong & Kim, 1997), water (Bokotko, et al, 2005) and seawater, which is a promising solution in marine applications. The main advantages of seawater are the availability and the fact that the acidified effluent can be discharged directly into the sea after a simple neutralization process (Pyszko, et al, 2015; Ammar & Seddiek, 2017). There are some reports about seawater scrubbers available in the literature. For instance, Zhang

et al (1988), Oikawa *et al.* (2003) and Williams (1999) analyzed seawater wet scrubbers used in power plants. Sun *et al.* (2008) showed that the mass transfer coefficient in seawater is about twice as great as that of the NaOH solution with pH 8.35. Darake *et al.* (2014) carried out an experimental study and mathematical modeling about SO_2 removal by seawater in a packed-bed tower. Caiazzo *et al*. (2013) analyzed a seawater spray scrubber operating under marine diesel exhaust conditions and compared seawater to distilled water. Sukheon and Nishida (2003) analyzed the effect of seawater under SO_x, particulate matter, CO_2 and NO_x.

The complexity of the SO_2 absorption process makes it difficult to analyze through theoretical or experimental analyses. In the recent years, the development of computer technology has become numerical procedures an important tool to predict the droplet absorption process. Most of the numerical work available in the literature refers to simulations of the whole geometry of scrubbers. Instead the whole scrubber, the analysis of a single droplet provides information about diffusion, convection inside the droplet, or evaporation. There are several papers that analyze single liquid droplets in the literature, most of them focused on SO_2 scavenging by rainwater in the atmosphere. For instance, Babolal *et al.* (1981) studied atmospheric SO_2 scavenged by water drops by means of a simple numerical method. Huckaby and Ray (1989) analyzed numerically the absorption of SO_2 by a stationary water droplet under condensation or evaporation and, more recently, Chen *et al*. (Chen, 2001 & 2006, Chen, et al, 2011 and Chen, et al, 2012) developed a CFD model to analyze SO_2 reduction by water droplets in the atmosphere analyzing both liquid droplets and gas medium.

The purpose of this paper is to develop a numerical model to analyze SO_2 absorption by seawater and continue the work developed elsewhere (Lamas et al, 2016). To this end, a moving water droplet immersed in a gas medium was analyzed. Both liquid and gas phases were included in the model. The proposed CFD model takes in consideration the fluid motion inside and outside the droplet, heat transfer, chemical reactions and mass diffusion.

2. NUMERICAL IMPLEMENTATION

The model proposed in the present paper analyzes the amount of SO_2 absorbed by a single droplet which falls counter flow with respect to an exhaust gas stream with SO_2. The computational domain is indicated in Figure. 2. As can be seen, the domain size is 15 x 6 droplet radii from the droplet center since it was verified that these dimensions eliminate any potential effect of the outer boundaries on the flow close to the droplet. Several tests were performed in order to set the more appropriate dimension of the computational domain. The problem was simulated as axisymmetric.

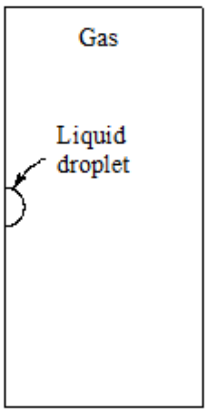

Figure 2. Computational domain.

When viewed in a fixed coordinate system, the droplet and gas move relatively with each other. Modeling this movement requires a large domain and thus high computational time. An alternative approach is to work using a coordinate system which moves with the droplet. In this case, the droplet is fixed in space and the relative droplet-gas velocity is imposed as inlet and outlet boundary conditions, *i.e.*, the gas flow enters and leaves the computational domain at the relative velocity. This velocity is variable due to the effects of buoyancy and drag. Buoyancy tends to accelerate the droplet, while drag tends to decelerate it.

2.1 CHEMICAL MODEL

The principle of operation of a seawater scrubber is based on a spray of droplets which fall counter flow to an exhaust gas containing SO_2. When the gas is in touch with a droplet, the concentration at the interface follows the Henry's law. A concentration gradient is induced in the interface and SO_2 is transported into the droplet by mass diffusion according to the Fick's law. Chemical dissociation reactions also take place inside the droplet.

While several alkaline species are presented in seawater (HCO_3^-, CO_3^{2-}, $B(OH)_4^-$, OH^-, HPO_4^{2-}, etc), the main contribution to alkalinity is by far the bicarbonate ion HCO_3^-, and typical concentrations are 2,400µmol/kg of H_2O (Sverdrup, et al, 1942; Dickson & Goyet, 1994 & Andreason & Mayer, 2007).

Regarding chemical reactions, the model proposed by Andreasen and Mayer (2007) was adopted. This assumes the following chemical reactions:

$$SO_2(g) \leftrightarrow SO_2(aq) \quad (1)$$

$$SO_2(aq) + 2H_2O(l) \leftrightarrow HSO_3^-(aq) + H_3O^+(aq) \quad (2)$$

$$HSO_3^-(aq) + H_2O(l) \leftrightarrow SO_3^{2-}(aq) + H_3O^+(aq) \quad (3)$$

$$HCO_3^-(aq) + H_3O^+(aq) \leftrightarrow CO_2(aq) + 2H_2O(l) \quad (4)$$

$$CO_2(aq) \leftrightarrow CO_2(g) \quad (5)$$

Reaction (1) represents the dissolution of gaseous SO_2 in water at the liquid-gas interphase, and it is governed by Henry's law:

$$[SO_2(aq)] = p_{SO_2} k_H \tag{6}$$

where p_{SO2} is the partial pressure of SO_2, $[SO_2(aq)]$ the concentration of SO_2 in the solution and k_H the Henry's constant, expressed as (Sander, 2005):

$$k_H = k_H^0 e^{\frac{-\Delta H_{soln}}{R}\left(\frac{1}{T}-\frac{1}{T^0}\right)} \tag{7}$$

where k_H^0 is the Henry's constant at the reference state, ΔH_{soln} the enthalpy of solution, T the temperature in Kelvin and T^0 the reference state temperature (298.15 K). A value of k_H^0 = 1.2 mol/(kg atm) and the slope $-\Delta H_{soln}/R$ = 2850 K were employed, Sander (2005).

Reaction (5) represents the dissolution of CO_2 at the liquid-gas interphase. This is also governed by Henry's law.

Reactions (2-4) occur inside the droplet and their kinetics was assumed to be in equilibrium (Chen, et al, 2011 & Andreason, 2007). The equilibrium condition was imposed by minimizing the Gibbs free energy according to the mass action law. Reactions (2-4) can be written in general form as follows:

$$aA + bB \leftrightarrow cD + dD \tag{8}$$

where A and B are reactants, C and D products, and a, b, c, and d the stoichiometric coefficients. According to the mass action law, the Gibbs free energy is minimum when:

$$-\frac{\Delta G_0}{RT} = ln\left(\frac{[C]^c[D]^d}{[A]^a[B]^b}\right) \tag{9}$$

where ΔG^0 is the standard Gibbs free energy change, R the universal gas constant, [A] the molar concentration of species A at equilibrium, and so forth. The term $[C]^d[D]^d/([A]^a[b]^b)$ is the so-called equilibrium constant for the reaction.

2.2 GOVERNING EQUATIONS

The governing equations are the transport equations of conservation of mass, momentum and energy, Eqs. (10-12) respectively. A laminar simulation was carried out due to the low droplet diameters and velocities employed. Inside the droplet, the energy equation was solved until the evaporation temperature was reached. From this temperature, it was imposed as constant and a diameter reduction due to evaporation was implemented in the code.

$$\nabla \cdot \vec{u} = S_m \tag{10}$$

$$\rho \frac{\partial \vec{u}}{\partial t} + \rho \nabla \cdot (\vec{u}\vec{u}) = -\nabla p + \rho \vec{g} - \nabla \cdot \tau + S_{mo} \tag{11}$$

$$\rho c \frac{\partial T}{\partial t} + \rho c \nabla \cdot (\vec{u}T) = k \nabla^2 T + S_e \tag{12}$$

In the equations above, u is the velocity, ρ the density, t the time, p the pressure, τ the stress tensor, c the specific heat and k the thermal conductivity. The terms S_m, S_{mo} and S_e are sources in the equations of mass, momentum and energy respectively.

The source term S_m of Eq. (10) accounts for the phase change, and is given by (Sim, et al, 2015):

$$S_m = \left(\frac{1}{\rho_v} - \frac{1}{\rho_l}\right) m \tag{13}$$

where $m = \nabla H h (T_e - T_g)/h_{lv}$ and the term $h(T_e - T_g)$ represents the heat transferred between the droplet and gas. Therefore, $h(T_e - T_g)/h_{lv}$ is the mass transfer per unit area along the interface. T_e is the evaporation temperature, T_g the gas temperature, h_{lv} the latent heat of evaporation, and h the heat transfer coefficient, given by the Ranz-Marshall equation (Ranz & Marshall, 1952):

$$\frac{hD}{k} = 2 + 0.6\,\mathrm{Re}^{1/2}\,\mathrm{Pr}^{1/3} \tag{14}$$

where k is the thermal conductivity, Re the Reynolds number, Pr the Prandtl number and D the droplet diameter. In the present work the shape of the droplet remained practically spherical due to the importance of the surface tension force in comparison with the inertial force.

H is the so-called Heaviside function. In the present paper, this takes a 0 value for the liquid, 1 for the vapor and a value between 0 and 1 along the interface, Eq. (15).

$$H = \begin{cases} 0 & \text{if } \phi < \varepsilon \\ 1 & \text{if } \phi > \varepsilon \\ (\phi + \varepsilon)/(2\varepsilon) + [\sin(\pi\phi/\varepsilon)]/(2\pi) & \text{if } |\phi| \le \varepsilon \end{cases} \tag{15}$$

where ε is a small quantity of the order of the mesh size.

The source term S_e indicated in Eq. (12) also accounts for the phase change, and is given by:

$$S_e = h_{lv} m \tag{16}$$

The source term S_{mo} of Eq. (11) accounts for the effect of surface tension, given by (Brackbill, et al, 1992):

$$S_{mo} = \sigma \kappa \nabla H \tag{17}$$

where κ is the curvature of the interface.

The interface was treated using the level set method. This procedure consists on assigning a scalar magnitude, the level set ϕ, to the distance from the interface. The interface corresponds to a zero value of the level set. In the present work, a negative sign of ϕ was adopted for the vapor and positive for the liquid. The propagation of the interface is provided by the following equation:

$$\frac{\partial \phi}{\partial T} + \vec{u}_{\text{int}} \cdot \nabla \phi = 0 \tag{18}$$

Where $\vec{u}_{\text{int}}$ is the velocity of the interface, which can be obtained by a mass and heat transfer balance at the interface, given by:

$$\vec{m} = \frac{h(T_e - T_g)}{h_{lv}} = \rho(\vec{u}_{\text{int}} - \vec{u}) \tag{19}$$

In order to preserve the property of being distance from the interface, the level set function must be reinitialized at each time step through the following equation:

$$\frac{\partial \phi}{\partial \xi} = sign(\phi_0)(1 - |\nabla \phi|) \tag{20}$$

where ξ is an artificial time introduced because Eq. (20) is a temporal equation which must be solved at each time step, and ϕ_0 the level set field at the start of each iteration in this artificial time, *i.e.*:

$$\phi(x,0) = \phi_0(x) \tag{21}$$

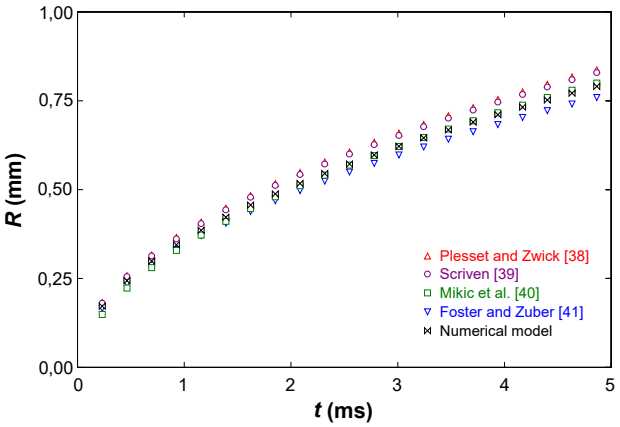

Figure 3. Bubble radius applied to a spherical water bubble growing in a 5ºC superheated liquid medium.

The accuracy of the evaporation model was validated with experimental results elsewhere (Lamas, 2012; Lamas, et al, 2012; and Lamas, et al, 2015). Several authors reported results about spherical bubble growing due to evaporation (Plesset & Zwick, 1954; Scriven, 1959; Mikic, et al, 1970; and Foster & Zuber, 1954) and developed correlations based on their experimental findings. As comparison between these correlations proposed in the literature and the results proposed by the present numerical model, Figure. 3 shows the evolution of the bubble radius against time for a spherical bubble of water immersed in a liquid medium 5ºC superheated. As can be seen in this figure, the developed numerical model provides reasonable results.

2.3 BOUNDARY CONDITIONS

As mentioned previously, a reference frame which moves with the droplet was employed. A free-stream velocity was imposed as inlet and outlet boundary conditions. The drag force decelerates the relative velocity between the droplet and gas, while buoyancy accelerates it. This was implemented into the numerical model by adjusting the free-stream velocity at each time step. The acceleration or deceleration is given by:

$$\frac{du_\infty(t)}{dt} = g - \frac{F_{drag}}{\rho_l \pi D^3 / 6} \tag{22}$$

where u_∞ is the free-stream velocity and F_{drag} the drag force, given by:

$$F_{drag} = \frac{C_D A_f \rho_g (u_\infty + u_g)^2}{2} \tag{23}$$

where u_g is the gas velocity, A_f the reference area (for a sphere $\pi D^2/4$), and C_D the drag coefficient, obtained by the following expression (Seinfeld, 1986):

$$C_D = \frac{24}{\text{Re}}\left(1 + 0.15\,\text{Re}^{0.687}\right) \tag{24}$$

Finally, the variation of the free-stream velocity during a time step Δt is:

$$u_\infty(t + \Delta t) = u_\infty(t) + \Delta t \frac{du_\infty(t)}{dt} \tag{25}$$

2.4 CFD MODEL

The computational mesh is indicated in Figure. 4. The problem was simulated using the open software OpenFOAM (Open Field Operation and Manipulation). This software was chosen because it allows a total manipulation of the code. A new OpenFOAM solver was programmed for the present study. C++ programming language was employed to write it.

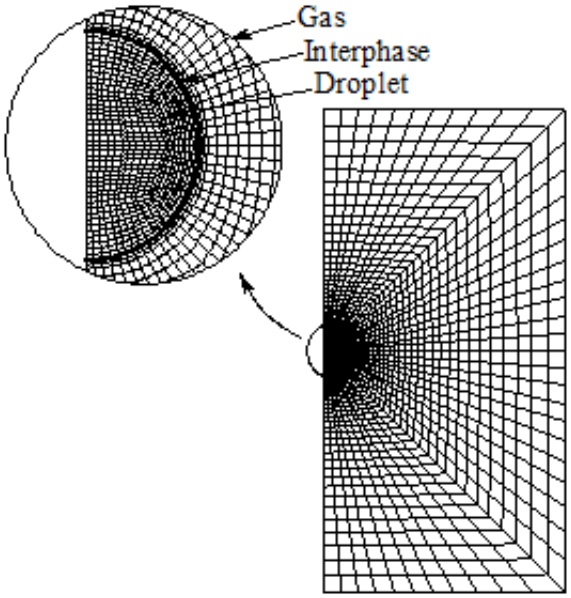

Figure 4. Computational mesh.

As indicated previously, several tests were performed in order to determine the adequate extent of the numerical domain in such a way to eliminate any potential effect of the outer boundaries (theoretically at infinity) on the flow close to the droplet. In addition, the solution was checked for refinement sensibility on both the mesh size and time step. Four meshes and time steps were tested to verify that the results are independent of these parameters. The number of elements of these meshes was 1414 (Mesh 1), 1821 (Mesh 2), 2112 (Mesh 3), and 2412 (Mesh 4), while the time steps were $2.5 \cdot 10^{-4}$ s (Time step 1), $5 \cdot 10^{-5}$ s (Time step 2), 10^{-5} s (Time step 3), and $2 \cdot 10^{-6}$ s (Time step 4). The SO_2 absorbed by a droplet is indicated in Table 1. As can be seen, the results using Mesh 3 and Time step 3 are appropriate as refining mesh size or time step does not modify the error obtained. Therefore, Mesh 3 and Time step 3 were chosen for the present work.

Table 1. S absorbed by a droplet (mol/droplet) using several mesh sizes and time steps. 200 µm initial droplet diameter, 600 ppm SO_2 concentration, 2,400µmol/kg alkaline concentration, 400ºC initial gas temperature and 20ºC initial droplet temperature.

	Time step 1	**Time step 2**	**Time step 3**	**Time step 4**
Mesh 1	$1.62 \cdot 10^{-14}$	$1.67 \cdot 10^{-14}$	$1.69 \cdot 10^{-14}$	$1.73 \cdot 10^{-14}$
Mesh 2	$1.65 \cdot 10^{-14}$	$1.73 \cdot 10^{-14}$	$1.77 \cdot 10^{-14}$	$1.77 \cdot 10^{-14}$
Mesh 3	$1.73 \cdot 10^{-14}$	$1.77 \cdot 10^{-14}$	$1.77 \cdot 10^{-14}$	$1.77 \cdot 10^{-14}$
Mesh 4	$1.71 \cdot 10^{-14}$	$1.77 \cdot 10^{-14}$	$1.77 \cdot 10^{-14}$	$1.77 \cdot 10^{-14}$

The pressure-velocity coupling was treated using the PISO (Pressure Implicit Splitting of Operators) procedure. The equations were discretized by the QUICK interpolation and the temporal treatment was solved by an implicit method.

3. RESULTS

The numerical model developed in the present work was employed to study the influence of several parameters such as the droplet diameter, SO_2 concentration, alkalinity and temperature. The ranges analyzed correspond to typical concentrations obtained in diesel engine exhaust when burning heavy fuel oil (Kuiken, 2008; Woodyard, 2009; Lamas & Rodriguez, 2012; and Lamas & Rodriguez, 2018). Results are indicated below.

3.1 EFFECT OF THE INITIAL DROPLET DIAMETER

Figure. 5 shows the mass fraction of HCO_3^- overlaid with the velocity field for 0.5s using 600ppm SO_2 concentration (0.00133 kg of SO_2/kg of H_2O), 2,400µmol/kg alkaline concentration (0.000146 kg of alkaline/kg of H_2O), free stream initial velocity 2m/s (1 m/s liquid droplet velocity and 1m/s gas flow velocity), 400ºC initial gas temperature, 20ºC initial liquid temperature and 1,000µm initial droplet diameter. This figure shows that an internal vortex is formed due to drag and HCO_3^- is consumed first at the interphase and then at the core of the droplet. SO_2 first accumulates at the droplet surface and then is transported from the interface to the core of the droplet by three mechanisms: radial diffusion, internal circulation and chemical reactions.

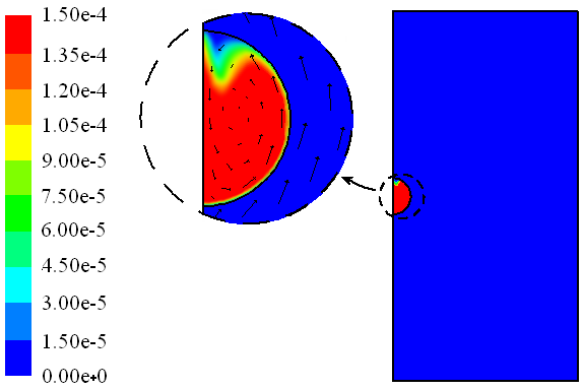

Figure 5. Mass fraction of HCO_3^- overlaid with velocity field.

Figure. 6 indicates the droplet diameter reduction for 1,000, 500 and 200µm initial diameters. As expected, all droplets experiment a reduction of the diameter due to the evaporation effect implemented in the model. The time was represented between 0 and 3 seconds because

this is a reasonable value of residence time in scrubbers (Lamas, et al, 2016). The droplet velocity and position for these initial diameters are indicated in Figures. 7 and 8 respectively. Figures. 6-8 correspond to 600ppm SO_2 concentration, 2,400µmol/kg alkaline concentration, free stream initial velocity 2m/s, 400ºC initial gas temperature and 20ºC initial droplet temperature. As expected, lower diameters correspond to lower velocities. As indicated above, two effects are responsible for the droplet trajectory: buoyancy and drag. Larger droplets are associated to high gravity forces and thus to high velocities. Nevertheless, as the droplet diameter is reduced, buoyancy becomes less important and velocity tends to decay. As indicated below, 1 m/s was assumed for the droplet and 1 m/s for the gas. Figure. 7 indicates that all droplets depart from this initial velocity of 1 m/s and the largest droplet increments this velocity due to the importance of buoyancy, while the droplets of 500 and 200µm reduce this initial velocity due to the importance of drag.

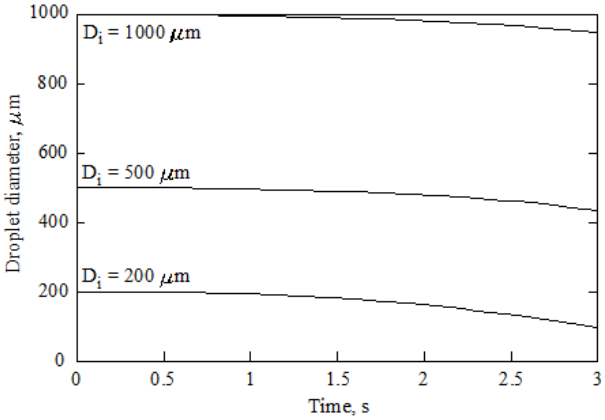

Figure 6. Droplet diameter against time. 600ppm SO_2 concentration, 2,400µmol/kg alkaline concentration, 400ºC initial gas temperature and 20ºC initial droplet temperature.

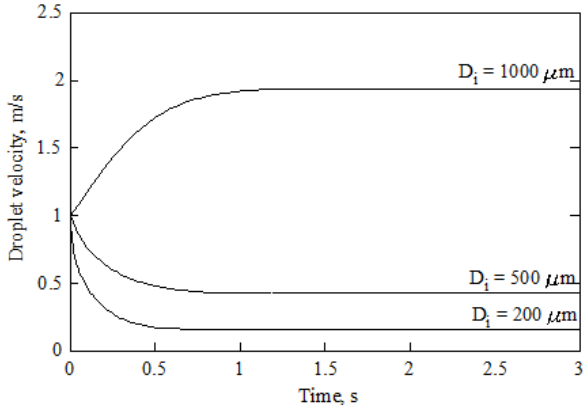

Figure 7. Droplet velocity against time. 600ppm SO_2 concentration, 2,400µmol/kg alkaline concentration, 400ºC initial gas temperature and 20ºC initial droplet temperature.

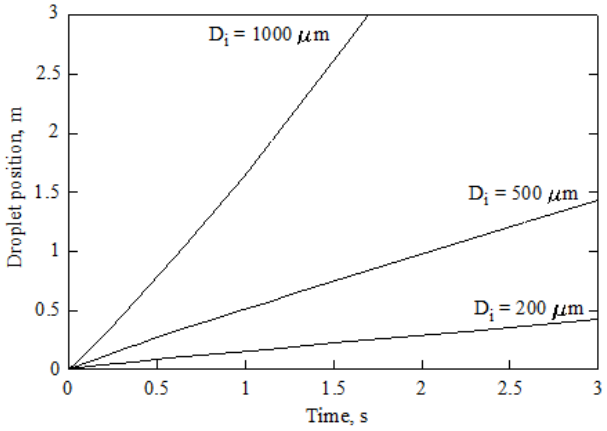

Figure 8. Droplet position against time. 600ppm SO_2 concentration, 2,400µmol/kg alkaline concentration, 400ºC initial gas temperature and 20ºC initial droplet temperature.

The quantity of sulphur (S) absorbed by each droplet is indicated in Figure. 8. The absorbed S was computed as the sum of moles of SO_2, HSO_3^- and SO_3^{2-}. As can be seen, larger droplets are associated to higher S absorption rates. Nevertheless small droplets are associated to lower S absorption rates. The reason is simply that the volume is lower. The main advantage of small droplets is that these reach the saturation state in less time due to a more efficient contact with the liquid. In practical applications, this fact promotes small scrubbers.

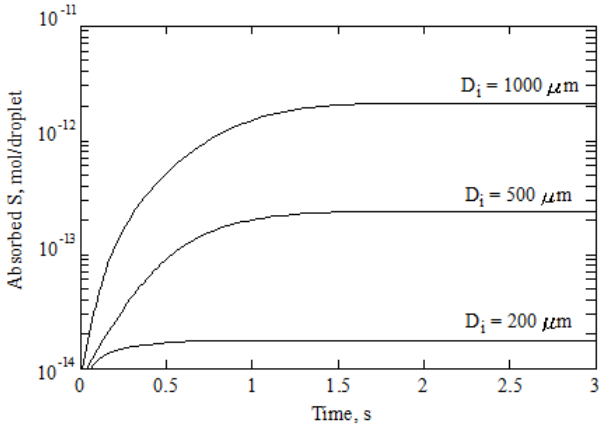

Figure 9. S absorbed by a droplet for several initial diameters. 600ppm SO_2 concentration, 2,400µmol/kg alkaline concentration, 400ºC initial gas temperature and 20ºC initial droplet temperature.

3.2 EFFECT OF THE SO_2 INITIAL CONCENTRATION

Figure. 10 indicates the S absorbed by a droplet against time for several initial SO_2 concentrations. This figure corresponds to 200µm initial droplet diameter, 2,400µmol/kg alkaline concentration, free stream initial

velocity 2m/s, 400ºC initial gas temperature and 20ºC initial droplet temperature. Three initial SO_2 concentrations were analyzed: 1,000, 750 and 600ppm. As can be seen, high SO_2 concentrations promote S absorption, and a 21.5% increment in the absorbed S was obtained from 600ppm to 1,000ppm.

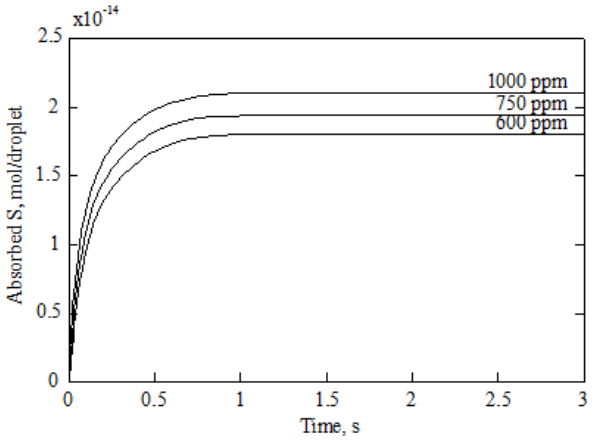

Figure 10. S absorbed by a droplet for several SO_2 initial concentrations. 200µm initial droplet diameter, 2,400µmol/kg alkaline concentration, 400ºC initial gas temperature and 20ºC initial droplet temperature.

3.3 EFFECT OF THE ALKALINITY

Figure. 11 indicates the S absorbed by a droplet against time for several alkaline concentrations. This figure corresponds to 200µm initial droplet diameter, 600ppm SO_2 concentration, free stream initial velocity 2m/s, 400ºC initial gas temperature and 20ºC initial droplet temperature. As can be seen, as alkalinity is increased SO_2 absorption is increased too, and a 19.8% increment in the absorbed S was obtained from 2,400µmol/kg to 5,000 µmol/kg.

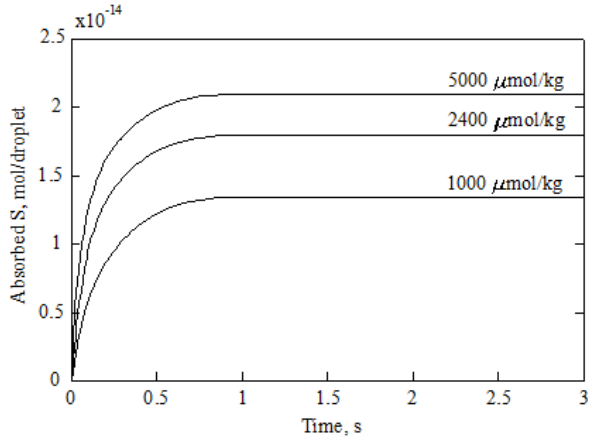

Figure 11. S absorbed by a droplet for several initial alkalinities. 200µm initial droplet diameter, 600ppm SO_2 concentration, 400ºC initial gas temperature and 20ºC initial droplet temperature.

3.4 EFFECT OF THE TEMPERATURE

Figure. 12 indicates the S absorbed by a droplet against time for several initial droplet temperatures. This figure corresponds to 200µm initial droplet diameter, 2,400µmol/kg alkaline concentration, 600ppm SO_2 concentration, free stream initial velocity 2m/s and 400ºC initial gas temperature. As can be seen, S absorption is improved when the droplet temperature is decreased, and a 2.2% variation in the absorbed S was obtained from 20ºC to 60ºC. The reason is that the concentration of SO_2 at the interphase is higher due to a higher value of the Henry's constant, indicated by Eq. (7).

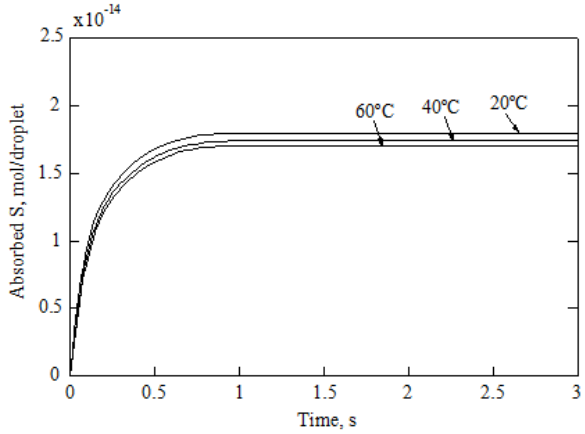

Figure 12. S absorbed by a droplet for several initial droplet temperatures. 200µm initial droplet diameter, 2,400µmol/kg alkaline concentration, 600ppm SO_2 concentration and 400ºC initial gas temperature.

Figure. 13 indicates the influence of the gas temperature. As can be seen, higher gas temperatures reduce S absorption, and a 16.3% variation in the absorbed S was obtained from 400ºC to 500ºC. The effect is more important than raising the droplet temperature. The reason is that higher gas temperatures induce higher interphase temperatures and thus lower SO_2 concentrations at the interphase.

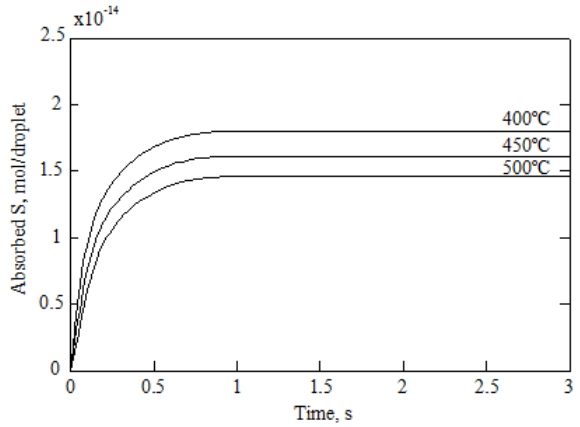

Figure 13. S absorbed by a droplet for several initial gas temperatures. 200µm initial droplet diameter, 2,400µmol/kg alkaline concentration, 600ppm SO_2 concentration and 20ºC initial droplet temperature.

4. CONCLUSIONS

This paper proposes a numerical model to analyze SO_2 absorption in seawater. SO_2 scrubbers allow employing high-sulphur fuels with a low impact on sulphur emissions. In marine applications, seawater is a promising solution due to its availability. This paper proposes a numerical model to analyze SO_2 absorption in seawater. A single seawater droplet was analyzed, and the developed model was used to predict the influence of several parameters on the desulphurization efficiency, such as the droplet diameter, SO_2 concentration, alkalinity and temperature. Several tests were carried out using typical exhaust conditions of marine engines. It was found that a droplet of 200 μm initial diameter can absorb $1.77 \cdot 10^{-14}$ mol of S for the parameters analyzed, and this reduction improves when the alkalinity and SO_2 concentration are increased and diameter, seawater temperature and gas temperature are reduced. Differences up to of 21.5%, 19.8%, 2.2% and 16.3% in the S reduction were obtaining varying the SO_2 initial concentration, alkaline initial concentration, initial liquid temperature and initial gas temperature respectively.

5. ACKNOWLEDGEMENTS

The authors would like to express their gratitude to "Talleres Pineiro, S.L.", sale and repair of marine engines.

6. REFERENCES

1. LAMAS, M.I., RODRIGUEZ, C.G., RODRIGUEZ, J.D., TELMO, J. *Internal modifications to reduce pollutant emissions from marine engines. A numerical approach*. Journal of Naval Architecture and Marine Engineering 5(4), 493-501, 2013. doi: 10.2478/IJNAOE-2013-0148.
2. LAMAS, M.I., RODRIGUEZ, C.G., TELMO, J., RODRIGUEZ, J.D. *Numerical analysis of emissions from marine engines using alternative fuels.* Polish Maritime Research 22(4), 48-52, 2015. doi: 10.1515/pomr-2015-0070.
3. LAMAS, M.I., RODRIGUEZ, C.G. *Numerical model to analyze NOx reduction by ammonia injection in diesel-hydrogen engines.* International Journal of Hydrogen Energy 42, 26132-26141, 2017. doi: 10.1016/j.ijhydene.2017.08.090.
4. LAMAS, M.I., RODRIGUEZ, C.G. *Numerical model to study the combustion process and emissions in the Wärtsilä 6L 46 four-stroke marine engine*. Polish Maritime Research 20(2), 61-66, 2013. doi: 10.2478/pomr-2013-0017.
5. SEDDIEK, I.S., ELGOHARI, M.M. *Eco-friendly selection of ship emissions reduction strategies with emphasis on SOx and NOx emissions*. International Journal of Naval Architecture and Ocean Engineering, 6, 737-748, 2014. doi: 10.2478/IJNAOE-2013-0209.
6. BARBOOTI, M.M., IBRAHEEM, N.K., ANKOSH, A.H. *Removal of nitrogen dioxide and sulphur dioxide from air streams by absorption in urea solution*. Journal of Environmental Protection 2, 6-14, 2011. doi: 10.4236/jep.2011.22020.
7. HIKITA, H., ASAI, S., TSUJI, T. *Absorption of sulfur dioxide into aqueous sodium hydroxide and sodium sulfite solutions.* AICHE Journal. 23, 538-544, 1977. doi: 10.1002/aic.690230419.
8. LANCIA, A., MUSMARRA, D., PEPE, F. *Modeling of SO_2 absorption into limestone suspensions*. Industrial & Engineering Chemical Research 36, 197-203, 1997. doi: 10.1021/ie9602365.
9. PUSKAR, M., BIGOS, P., BALAZIKOVA, M., PETKOVA, V. *The measurement method solving the problems of engine output characteristics caused by change in atmospheric conditions on the principle of the theory of optimal temperature range of exhaust system.* Measurement: Journal of the International Measurement Confederation 46, 467-475, 2013.
10. JEONG, S.M., KIM, S.D. *Enhancement of the SO_2 sorption capacity of CuO/γ-Al_2O_3 sorbent by an alkali-salt promoter*. Industrial & Engineering Chemical Research. 36, 5425-5431, 1997. doi: 10.1021/ie970206h.
11. BOKOTKO, R.P., HUPKA, J., MILLER, J.D. *Flue gas treatment for SO_2 removal with air-sparged hydrocyclone technology.* Environmental Science and Technology. 39, 1184-1189, 2005. doi: 10.1021/es035044x.
12. PYSZKO, R., BRESTOVIC, T., JASMINKA, N., LAZAR, M., MACHU, M., PUSKAR, M., TURISOVA, R. *Measuring temperature of the atmosphere in the steelmaking furnace.* Journal of the International Measurement Confederation 75, 92-103, 2015. doi: 10.1016/j.measurement.2015.07.052.
13. AMMAR, N.R., SEDDIEK, I.S. *Eco-environmental analysis of ship emission control methods: Case study RO-RO cargo vessel*. Ocean Engineering 137, 166-173, 2017. doi: 10.1016/j.oceaneng.2017.03.052
14. ZHANG, D.N., CHEN, Q.Z., ZHAO, Y.X., MAEDA, Y., TSUJINO, Y. *Stack gas desulfurization by seawater in Shanghai*. Water Air and Soil Pollution 130, 271-276, 2001. doi: 10.1080/08940630.1988.10466438.
15. OIKAWA, K., YONGSIRI, C., TAKEDA, K., HARIMOTO, T. *Seawater flue gas desulfurization: its technical implications and performance results.* Environmental Progress 22, 67-73, 2003. doi: 10.1002/ep.670220118.
16. WILLIAMS, P.J. *Use of seawater as makeup water for wet flue gas desulfurization systems*.

EPRI-DOE-EPA Comb. Utility air Poll. Control Symp. Atlanta, Georgia, USA, 1999.

17. SUN, X., MENG, F., YANG, F. *Application of seawater to enhance SO_2 removal from simulated flue gas through hollow fiber membrane contactor.* Journal of Membrane Science. 312, 6-14, 2008. doi: 10.1016/j.memsci.2007.12.011.
18. DARAKE, S., RAHIMI, A., HATAMIPOUR, M.S., HAMZELOUI, P. *SO_2 removal by seawater in a packed-bed tower: experimental study and mathematical modelling*. Separation Science and Technology. 49, 988-998, 2014. doi: 10.1080/01496395.2013.872660.
19. CAIAZZO, G., LANGELLA, G., MICCIO, F., SCALA, F. *An experimental investigation on seawater SO_2 scrubbing for marine application.* Environmental Progress & Sustainable Energy. 32, 1179-1186, 2013. doi: 10.1002/ep.11723.
20. SUKHEON, A., NISHIDA, O. *New application of seawater and electrolyze seawater in air pollution control of marine diesel engine*. JMSE International Journal, Series B: Fluids and Thermal Engineering. 46, 206-213, 2003. doi: 10.1299/jsmeb.46.206.
21. BABOOLAL, L.B., PRUPPACHER, H.R., TOPALIAN, J.H. *A sensitivity study of a theoretical model of SO_2 scavenging by water drops in air.* Journal of the Atmospheric Sciences 38, 856-870, 1981. doi: 10.1175/1520-0469.
22. HUCKABY, J.L., RAY, A.K. *Absorption of sulphur dioxide by growing and evaporating water droplets.* Chemical Engineering Science. 44, 2797-2808, 1989. doi: 10.1016/0009-2509(89)85089-4.
23. CHEN, W.H. *Unsteady absorption of sulfur dioxide by an atmospheric water droplet with internal circulation*. Atmospheric Environment. 35, 2375-2393, 2001. doi: 10.1016/S1352-2310(00)00536-7.
24. CHEN, W.H. *Air pollutant absorption by single moving droplets with drag force at moderate Reynolds numbers*. Chemical Engineering Science. 61, 449-458, 2006. doi: 10.1016/j.ces.2005.07.016.
25. CHEN, W.H., CHEN, Y.Y., HUNG, C.I. *A simplified model of predicting SO_2 absorption by single atmospheric raindrops with chemical dissociation and internal circulation*. Aerosol and Air Quality Research. 11, 860-872, 2011. doi: 10.4209/aaqr.2011.08.0130.
26. CHEN, W.H., CHEN, Y.Y., HUNG, C.I. *Transient SO_2 uptake dynamics in an atmospheric water aerosol with internal circulation and chemical dissociation.* Journal of Atmospheric and Solar-Terrestrial Physics. 77, 67-77, 2012. doi: 10.1016/j.jastp.2011.11.010.
27. LAMAS, M.I., RODRIGUEZ, C.G., RODRIGUEZ, J.D., TELMO, J. *Numerical model of SO_2 scrubbing with seawater applied to marine engines.* Polish Maritime Research 2(90), 42-47, 2016. doi: 10.1515/pomr-2016-0019.
28. SVERDRUP, H.U., JOHNSON, M.W., FLEMING, R.H. *The Oceans Their Physics, Chemistry, and General Biology*; Prentice-Hall: New York, 1942.
29. DICKSON, A. G., GOYET, C. *Handbook of methods for the analysis of the various parameters of the carbon dioxide system in sea water, Version 2*, ORNL/CDIAC-74; U.S. Department of Energy: Washington, DC, 1994.
30. ANDREASEN, A., MAYER, S. *Use of seawater scrubbing for SO_2 removal from marine engine exhaust gas*. Energy & Fuels 21, 3274-3279, 2007. doi: 10.1021/ef700359w.
31. SANDER, R. Henry's Law Constants. In *NIST Chemistry Webbook*; NIST Standard Reference Database Number 69; Linstrom P. J., Mallard W. G., Eds.; National Institute of Standards and Technology: Gaithersburg, 2005.
32. SIM, J., IM, H.G., CHUNG, S.H. *A computational study of droplet evaporation with fuel vapor ejection induced by localized heat sources*. Physics of Fluids 27, 053302, 2015. doi: 0.1063/1.4919809.
33. RANZ, W.E., MARSHALL, W.R. *Evaporation from drops. Parts I & II*. Chemical Engineering Progress 48, 141-146, 173-180, 1952.
34. BRACKBILL, J.U.; KOTHE, D.B.; ZEMACH, C. *A continuum method for modeling surface tension*. Journal of Computational Physics, 100, 335-354, 1992.
35. LAMAS, M. I. *Study of the heat transfer related to bubbles in heated surfaces* (in Spanish). Ph. D. Thesis, Universidade da Coruña, Spain. 2012.
36. LAMAS, M.I., JABARDO, J.M.S., ARCE, A., FARIÑAS, P. *Numerical analysis of the bubble detachment diameter in nucleate boiling*. Journal of Physics: Conference Series 395(1), 012174, 2012.
37 LAMAS, M.I., FARIÑAS, P., ARCE, A., SANCHEZ, M.L. *A numerical evaluation of the contribution of different heat transfer mechanisms in nucleate boiling.* Journal of the Brazilian Society of Mechanical Sciences and Engineering 37, 1543-1553, 2015. doi: 10.1007/s40430-015-0321-9.
38. PLESSET, M.S., ZWICK, S.A. *The growth of vapor bubbles in superheated liquid*. Journal of Applied Physics 25, 493-500, 1954.
39. SCRIVEN, L.E. *On the dynamics of phase growth*. Chemical Engineering Science 10, 1–13, 1959.
40. MIKIC, B.B., ROHSENOW, W.M., GRIFFITH, P. *On bubble growth rates*.

International Journal of Heat and Mass Transfer 13, 657-666, 1970.

41. FOSTER, H.K., ZUBER, N. *Growth of vapor bubbles in superheated liquid*. Journal of Applied Physics 25, 474-478, 1954.
42. SEINFELD, J.H. *Atmospheric Chemistry and Physics of Air Pollution*. Wiley, New York, 1986.
43. KUIKEN, K. *Diesel engines for ship propulsion and power plants from 0 to 100,000kW.* 1st Edition. The Netherlands: Target Global Energy Training, 2008.
44. WOODYARD, D. *Pounder's marine diesel engines and gas turbines.* 9th Edition. Oxford. Elsevier, 2009.
45. LAMAS, M.I., RODRIGUEZ, C.G. *Emissions from marine engines and NOx reduction methods*. Journal of Maritime Research 9(1), 77-81, 2012.
46. LAMAS, M.I.; RODRIGUEZ, C.G. *Numerical model to analyze NOx reduction by ammonia injection in diesel-hydrogen engines*. International Journal of Hydrogen Energy 42, 26132-26141, 2018. doi: 10.1016/j.ijhydene.2017.08.090.

